Antiphase domain boundaries at the Fe_3O_4(001) surface

Gareth S. Parkinson,[1,*] Thomas A. Manz,[2] Zbyněk Novotný,[1] Phillip T. Sprunger,[3] Richard L. Kurtz,[3] Michael Schmid,[1] David S. Sholl,[2] and Ulrike Diebold[1]

[1]*Institute of Applied Physics, Vienna University of Technology, Vienna, Austria*

[2]*School of Chemical & Biomolecular Engineering, Georgia Institute of Technology, Atlanta, Georgia 30332-0100, USA*

[3]*Department of Physics and Astronomy, Louisiana State University, Baton Rouge, Louisiana 70803-4001, USA*

(Received 17 January 2012; published 24 May 2012)

Antiphase domain boundaries (APDBs) in the $(\sqrt{2} \times \sqrt{2})R45^\circ$ reconstruction of the Fe_3O_4(001) surface were investigated using scanning tunneling microscopy (STM) and density functional theory [(DFT) + U] calculations. The equilibrium structure of the APDBs is interpreted in terms of the distorted B-layer model for the $(\sqrt{2} \times \sqrt{2})R45^\circ$ reconstruction in which a lattice distortion couples to charge order in the subsurface layers. The APDBs are observed after prolonged annealing at 700 °C, indicating that they are extremely stable. DFT + U calculations reveal that the APDB structure is linked to a disruption in the subsurface charge-order pattern, leading to an enrichment of Fe^{2+} cations at the APDB. Simulated STM images reproduce the appearance of the APDBs in the experimental data and reveal that they are preferential adsorption sites for hydrogen atoms.

DOI: 10.1103/PhysRevB.85.195450 PACS number(s): 68.37.Ef, 68.47.Gh, 68.43.Bc

I. INTRODUCTION

Magnetite (Fe_3O_4) is a half metallic ferrimagnet with wide ranging applications in current and emerging technologies.[1,2] At room temperature, Fe_3O_4 crystallizes in the inverse spinel structure (AB_2O_4). This can be viewed as a face-centered-cubic (FCC) oxygen lattice with nominal Fe^{3+} cations occupying tetrahedral Fe(A) sites and a 1:1 mixture of Fe^{2+} and Fe^{3+} cations occupying 1/2 of the Fe(B) octahedral interstitial sites. However, the chemical formula is often written as $(Fe^{3+})(Fe^{2.5+},Fe^{2.5+})O_4^{2-}$ as significant electron delocalization occurs on the Fe(B) sublattice rendering all Fe(B) atoms equivalent [see Fig. 1(a)].

On cooling through 125 K, Fe_3O_4 undergoes the Verwey transition,[3,4] and the conductivity drops by 2 orders of magnitude. Originally, it was postulated that the Verwey transition was a consequence of long-range charge order on the Fe(B) cations, but more recent results have shown the situation to be more complex, and the finer details remain controversial.[4–8] An orthorhombic lattice distortion occurs, reducing the symmetry to monoclinic,[4,7,8] but while theoretical papers predict that charge order accompanies the lattice distortion,[9–12] there is currently no consensus concerning a model. Such studies are challenging due to the large number of atoms in the monoclinic unit cell (168) and strong electron correlation effects.

In recent years, it has been proposed that the $(\sqrt{2} \times \sqrt{2})R45^\circ$ reconstruction, commonly reported at the Fe_3O_4(001) surface, is the result of a lattice distortion and charge order on the Fe(B) sublattice,[13–15] bearing a similarity to the insulating phase below the Verwey transition temperature. A combined low-energy electron diffraction (LEED) I-V and DFT study determined a distorted B-layer termination to be energetically favorable across a wide range of oxygen chemical potentials[16,17] and proposed a structural model that was largely consistent with experimental data. The lattice distortion involves the lateral relaxation of alternate pairs of surface Fe(B) atoms in opposite directions perpendicular to the Fe(B) row [see Fig. 1(b)], doubling the periodicity along the row direction. The $(\sqrt{2} \times \sqrt{2})R45^\circ$ symmetry occurs [black square in Fig. 1(b)] as the relaxations in neighboring rows occur in antiphase. Atomically resolved scanning tunneling microscopy (STM) images clearly resolve the undulating rows of Fe(B) atoms.[18–22]

With a structural model in place, further theoretical calculations[13,14] were performed in an attempt to better model the electronic properties. DFT + U calculations in which the Hubbard U parameter is used to account for electron correlation find that the surface layer contains Fe^{3+}-like cations. This is consistent with angle-resolved x-ray photoemission spectroscopy measurements, which show the surface to be Fe^{3+} rich.[23,24] In the second B layer, pairs of Fe^{2+}-like and Fe^{3+}-like cations are distributed with the same $(\sqrt{2} \times \sqrt{2})R45^\circ$ symmetry as the lattice distortion in the surface layer [see Fig. 1(b), right-hand side].[13,14] The symmetry of the system precludes charge order in the third subsurface B layer as all Fe(B) atoms possess an equal number of Fe^{2+} and Fe^{3+} neighbors from the second layer. These electronic effects lead to a half metal-semiconductor transition at the surface as observed by scanning tunneling spectroscopy[25] where a band gap of 0.2 eV was measured.

In this paper, we investigate highly stable antiphase domain boundaries (APDBs) in the $(\sqrt{2} \times \sqrt{2})R45^\circ$ reconstruction of Fe_3O_4(001). The APDBs described here are distinct from those that form in the bulk structure of thin Fe_3O_4 films grown on MgO(001) (Refs. 26–29) as they exist only within the surface reconstruction. We show that the structure of the surface APDBs can be interpreted using the distorted B-layer model of the surface[13,14] assuming a preference for four Fe^{2+}-like cations to meet in the subsurface layer. DFT + U calculations based on the experimentally derived APDB structure and the distorted B-layer model correlate well with the experimental STM images and show that the APDB is a preferential adsorption site for hydrogen atoms.

II. EXPERIMENTAL AND COMPUTATIONAL METHODS

A. Scanning tunneling microscopy experiments

The experiments were performed in an ultrahigh vacuum system with separate vessels for preparation and analysis (base

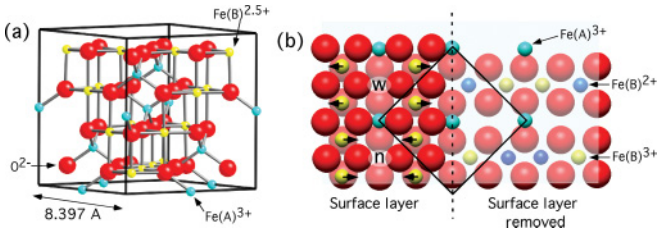

FIG. 1. (Color online) (a) Bulk unit cell for the room-temperature phase of Fe_3O_4. (b) Top view of the distorted B-layer model for the $(\sqrt{2}\times\sqrt{2})R45^\circ$ reconstructed $Fe_3O_4(001)$ surface. In the surface layer (left of the dashed line), pairs of surface Fe$(B)^{3+}$ cations relax perpendicular to the Fe(B) row direction producing inequivalent narrow "n" and wide "w" sections. In the second layer, a bimodal charge order exists with formal Fe$(B)^{2+}$ and Fe$(B)^{3+}$ cations underneath the surface oxygen in the narrow and wide regions of the unit cell, respectively.

pressures 1×10^{-10} and 5×10^{-11} mbar, respectively). A synthetic $Fe_3O_4(001)$ single crystal was prepared by 1-keV Ar^+ sputtering for 20 min (3 μA sample current) followed by annealing at 700 °C in an O_2 partial pressure of 2×10^{-6} mbar for 60 min. This procedure produces a sharp $(\sqrt{2}\times\sqrt{2})R45^\circ$ LEED pattern and no visible contamination in x-ray photoelectron spectroscopy as reported previously.[21,22,30] STM images of the sample surface were acquired using a SPECS Aarhus STM150 with electrochemically etched W tips. All STM images were acquired tunneling into empty states at room temperature with positive sample biases of 1–1.2 V and tunneling currents of 0.24–0.35 nA.

B. DFT + U computations

Since magnetite is a highly correlated material, an accurate exchange-correlation (XC) functional is required to compute its correct ground state. Common local spin-density approximation and generalized gradient approximation XC functionals overly delocalize electrons in many extended materials.[31–33] For large unit cells, an on-site energy correction is the most computationally feasible solution for this delocalization error. We used the formulation of Dudarev *et al.* for the DFT + U method, which depends on a single on-site parameter (U_{eff} value) for each atom.[34] In this method, the on-site energy correction is

$$E_{\text{correction}} = \frac{1}{2}\sum_A\sum_m U_{\text{eff}}^A\left[f_m^A-\left(f_m^A\right)^2\right], \qquad (1)$$

where U_{eff}^A is the U_{eff} value for atom A and $0\leqslant f_m^A\leqslant 1$ is the fractional occupation of the mth d orbital of atom A as determined by spherical harmonic projection.[34] (U_{eff} is zero for atoms such as hydrogen and oxygen that are not transition metals.) Since $f_m^A-(f_m^A)^2\geqslant 0$, positive U_{eff} values penalize fractional d-state occupation. Since the $Fe^{2.5+}$ oxidation state is associated with fractional d-state occupation, large U_{eff} values cause Fe(B) atoms to charge order into separate Fe^{2+} and Fe^{3+} sites. Specifically, when the same U_{eff} value is used for all Fe atoms in bulk magnetite, all Fe(B) atoms are equivalent when $0\leqslant U_{\text{eff}}<2.6$ eV but separate into distinct Fe^{2+} and Fe^{3+} sites when $U_{\text{eff}}>2.6$ eV.[35,36] Room-temperature bulk magnetite is not charge ordered, and each Fe(B) has an effective oxidation state of $+2.5$ with fractionally occupied d orbitals; consequently, $0\leqslant U_{\text{eff}}<2.6$ eV should be used for simulating bulklike magnetite layers at high temperatures.[36]

At first, it may appear logical to use the same U_{eff} value on all Fe atoms in slab models of the $Fe_3O_4(001)$ surface reconstruction, but a closer examination shows this is not optimal. Extensive tests we performed with different U_{eff} values clearly show the $Fe_3O_4(001)$ Jahn-Teller surface reconstruction occurs only when charge ordering in the first subsurface Fe(B) layer has alternating Fe^{2+} and Fe^{3+} pairs, which agrees with the charge ordering reported by Łodziana.[13] Moreover, we found that using small (e.g., 0 or 0.5 eV) U_{eff} values for Fe in all slab layers gives a ground state with no subsurface charge ordering and no surface reconstruction. We found that using large (e.g., $\geqslant$3.0 eV) U_{eff} values for Fe in all slab layers gives a ground state with poorly reproducible charge ordering in all subsurface layers. The charge ordering is poorly reproducible because of frustration between charge ordering in the bulklike (middle) slab layers and the first subsurface layer, leading to a multitude of local minima, which trap the charge ordering in nonequilibrium states. This suggests U_{eff} should be larger on the top two Fe(B) layers and smaller on the deeper Fe(B) layers to confine charge order to the first subsurface Fe(B) layer. It is well established that U_{eff} values increase in environments with lower conductivity and electrical screening.[33] The larger U_{eff} values near the $Fe_3O_4(001)$ surface have their physical origin in the surface's decreased conductivity and electrical screening relative to the deeper bulklike layers.

Thus far, we have considered the relationship between U_{eff} and charge ordering. We now consider the relationship between U_{eff} and Fe oxidation states. Van der Marel and Sawatzky used spectroscopic data of ions embedded in metallic hosts to generate semiempirical U_{eff} formulas for transition metals in various oxidation states.[33] These give $U_{\text{eff}}=1.13$ eV for Fe^{2+} and 6.31 eV for Fe^{3+}. The experimental value for the Fe(A) atomic spin moment (ASM) in the room-temperature phase of bulk magnetite is -3.82.[37] Earlier, we showed that using $U_{\text{eff}}=0$ underpredicts this ASM, whereas, using $U_{\text{eff}}=3.2$ overpredicts this ASM.[35] Using $U_{\text{eff}}=1.13$ eV for all Fe atoms in bulk magnetite with the Perdew-Burke-Ernzerhof XC functional, we obtain an Fe(A) ASM of -3.79 [density-derived electrostatic and chemical (DDEC) method][35,38] and -3.77 (Bader method),[39,40] suggesting this is a good U_{eff} value for modeling bulk magnetite near room temperature. We have, thus, used this value for all Fe atoms in the bulklike layers [i.e., deeper than the first subsurface Fe(B) layer] in our slab calculations.

For the surface and first subsurface Fe(B) layers, we used $U_{\text{eff}}=1.13$ eV for Fe^{2+} and 6.31 eV for Fe^{3+}. Since Fe(A) sites are not directly involved in charge ordering, we found U_{eff} for the near-surface Fe(A) sites was not critical and could be set to either 1.13 or 6.31 eV with similar results; $U_{\text{eff}}=1.13$ eV was used in our calculations. Because higher U_{eff} values increase the energy of partially occupied d states [Eq. (1)], leftover d electrons preferentially go to Fe(B) sites with $U_{\text{eff}}=1.13$ eV instead of those with $U_{\text{eff}}=6.31$ eV. Using this approach, Fe(B) sites with the Fe^{3+} oxidation state can be preselected

by setting $U_{\text{eff}} = 6.31$ eV on those atoms at the beginning of the calculation, allowing a particular charge-order pattern to be imposed on a slab before relaxation. This allows the calculation of nonminimum energy structures, such as an APDB, using a tractable 3×3 unit cell (369 atoms in total). Essentially, the slab converges to the optimum structure consistent with a prescribed charge-order pattern.

DDEC[35,38] and Bader[39,40] atomic population analyses were performed to determine net atomic charges and atomic spin moments for each DFT + U optimized geometry listed in the Supplemental Material.[41] For DDEC analysis, the most recent version (i.e., DDEC/$c3$) was used.[42] Bader charges were computed using the program of Tang *et al.*[43] The DDEC atomic charges were: (a) ca. -1.0 to -1.3 for oxygen atoms, (b) ca. $+0.5$ for adsorbed H atoms, (c) ca. $+1.8$ to $+2.0$ for Fe(A) and Fe(B) atoms with 3+ oxidation, (d) ca. $+1.6$ to $+1.7$ for Fe(B) atoms with 2.5+ oxidation, and (e) ca. $+1.5$ to $+1.6$ for Fe(B) atoms with a 2+ oxidation state. Because of partially covalent bonding between iron and oxygen atoms, the net atomic charges have smaller magnitudes than the oxidation states. The Bader charges did not clearly correlate with Fe oxidation states.

III. RESULTS

A. STM experiments

In Figs. 2(a)–2(c), we show three STM images acquired from the freshly prepared $Fe_3O_4(001)$ surface. Figure 2(a) shows an overview image with four distinct terraces. Steps with a height of 0.2 nm separate terraces on which the Fe(B) row direction rotates by 90°, consistent with single steps between adjacent B layers. On the lower terrace, a chain of bright protrusions runs from one step edge in the upper portion of the image to a second step in the lower portion of the image (arrows). This feature does not continue onto the higher terraces and does not appear to continue in the vicinity. The area contained within the yellow square, centered on a representative section of the row of protrusions, is shown in higher resolution in Fig. 2(b). In this smaller-scale image, the undulating rows associated with the $(\sqrt{2} \times \sqrt{2})R45°$ reconstruction are more clearly resolved, and the characteristic wide w and narrow n areas within the surface reconstruction[21,22] are marked. The $(\sqrt{2} \times \sqrt{2})R45°$ surface unit cell is indicated by the red square.

At first glance, the row of protrusions that span the center of the imaged area in Fig. 2(b) resemble those frequently observed at step edges on the $Fe_3O_4(001)$ surface [see Fig. 2(a), for example]. However, there is no change in apparent height over the row, and the Fe(B) row direction does not rotate by 90°. By drawing lines connecting the w sections of the surface reconstruction phase on each side of the row of protrusions (i.e., the yellow and cyan lines), it is evident that the $(\sqrt{2} \times \sqrt{2})R45°$ reconstruction is half a unit cell out of phase with the discontinuity marked by the row of bright protrusions. Consequently, in what follows, we will refer to these features as APDBs.

In Fig. 2(c), we show an atomically resolved image (5.3×5 nm^2) centered on a representative section of an APDB. By following the wide w and narrow n periodicities

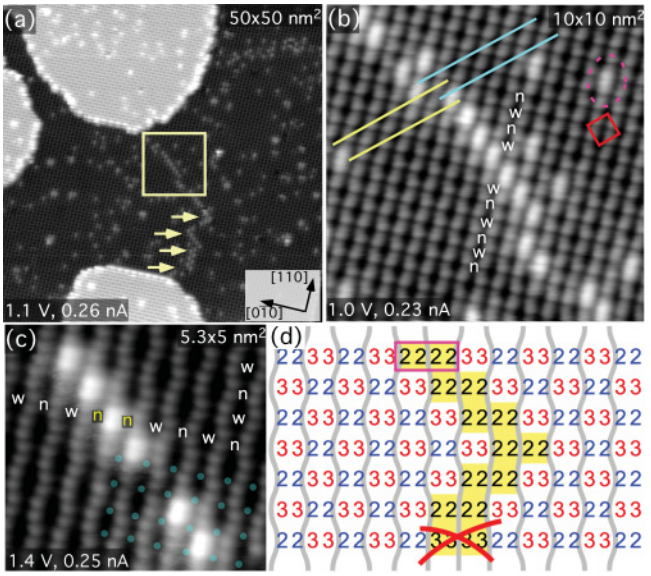

FIG. 2. (Color online) (a) Overview STM image of the as-prepared $Fe_3O_4(001)$ surface. A row of protrusions runs across the lower terrace terminating at step edges (indicated by the arrows). (b) High-resolution STM image of the area contained within the square in panel (a). On either side of the row of protrusions, the $(\sqrt{2} \times \sqrt{2})R45°$ reconstruction is out of phase by half a unit cell as indicated by the cyan and yellow lines, which pass through wide w sections of the reconstruction in each domain. Hydroxyl groups appear as bright protrusions on the Fe(B) rows (dashed oval). (c) Representative stretch of an APDB imaged with atomic resolution. Following the w and n sections of the surface reconstruction perpendicular to the Fe(B) row, it is clear that the APDBs are formed where two n sections meet. The circles indicate the position of the subsurface Fe(A) atoms with positions that are not affected by the APDB. The bright protrusions located at the APDB are due to adsorbed hydroxyl groups. (d) Schematic of the APDB structure assuming the distorted B-layer model of the $(\sqrt{2} \times \sqrt{2})R45°$ reconstruction. The undulating rows of surface Fe(B) atoms observed by STM are drawn as gray lines, whereas the subsurface Fe(B) atoms are indicated by 2 and 3 (their formal oxidation state). The scheme demonstrates that the n-n junction is consistent with four Fe^{2+} cations in a row in the second layer (highlighted yellow).

of the surface reconstruction perpendicular to the Fe(B) rows, one notices that the discontinuity in the phase of the surface reconstruction occurs with an n-n juncture, i.e., the surface reconstruction is narrow on either side of the protrusion. Analyzing many APDBs, we find that the formation of an APDB at the n-n junction is universally observed. The bright protrusions make it somewhat difficult to discern what happens at the junction along the Fe(B) row direction, but where a gap in the protrusions exists [one such gap is visible in Fig. 2(c)], it appears that the Fe(B) row runs straight over a four-atom section before the undulations of the surface reconstruction resume. Since the Fe(B) atoms within the rows are clearly visible in Fig. 2(c), the position of the subsurface Fe(A) atoms can be discerned utilizing the distorted B-layer model presented in Fig. 1(b). Drawing in these atoms (light blue circles), we see that the Fe(A) sublattice is continuous across the APDB. This demonstrates that the APDB occurs only in

the $(\sqrt{2} \times \sqrt{2})R45^\circ$ reconstruction and is not the result of a defect in the bulk structure.

Figure 2(d) shows a schematic of the APDB structure derived from the experimental images in which the undulating rows of Fe(B) atoms are drawn as gray lines. The yellow boxes encompass the n-n junction in each horizontal row; one such region is highlighted by the magenta rectangle. The numbers show the position and formal oxidation state of the second layer Fe(B) atoms, assuming the bimodal charge-order model for the reconstructed surface[13] [see Fig. 1(b)] also applies when an APDB is present. In this scheme, the formation of an APDB at the n-n junction disrupts the subsurface charge order, leading to a pair of Fe^{2+}-like cations on either side of the boundary, i.e., four Fe^{2+} cations in a row beneath the APDB. A preference for this APDB structure is consistent with the observation that the APDBs travel at 45° with respect to the Fe(B) rows and explains why the APDB can frequently change direction and turn by 90° (one such 90° turn is included in the schematic). If the meeting of two Fe^{3+} pairs was as likely as the meeting of two Fe^{2+} pairs, the APDB could travel along the Fe(B) row direction; this is not observed experimentally [indicated by the red cross in Fig. 2(d)].

Important information regarding the formation mechanism of the APDBs can be gleaned from samples prepared with lower annealing temperatures. In Fig. 3(a), we show an overview image (50×50 nm^2) of the Fe_3O_4(001) surface following Ar^+ sputtering and postannealing at 300 °C in an O_2 background pressure of 2×10^{-6} mbar for 20 min. This produces a surface with many small terraces, each exhibiting the $(\sqrt{2} \times \sqrt{2})R45^\circ$ reconstruction. Figure 3(b) shows a high-resolution image (14.2×19.2 nm^2) of two small terraces of equal height separated by a short distance. By drawing lines that pass through the wide sections of the surface reconstruction on each terrace [as was performed in Fig. 2(b)], it is clear that the surface reconstruction on these islands is out of phase by half a unit cell. Further annealing of the surface shown in Figs. 3(a) and 3(b) produces a flat surface with large terraces and APDBs.

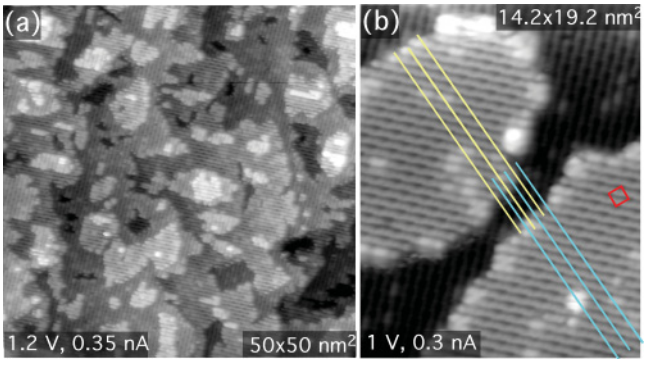

FIG. 3. (Color online) (a) STM image of the Fe_3O_4(001) surface following 1-keV Ar^+ sputtering (15 min) and 300 °C annealing (20 min) in a 2×10^{-6}-mbar O_2 background. Many small terraces are formed, in contrast to the samples annealed at 700 °C, which are largely flat (compare Fig. 2). (b) STM image of two small terraces that are not joined at any point. Lines connecting all of the wide sections of the lattice distortion on each terrace demonstrate that the terraces are out of phase by half a surface unit cell. The $(\sqrt{2} \times \sqrt{2})R45^\circ$ surface unit cell is indicated by the red square.

Based on Fig. 3, we propose that APDBs form on Fe_3O_4(001) when terraces with an out-of-phase lattice distortion coalesce. This assumes, however, that the surface reconstruction persists at annealing temperatures. To investigate this, we monitored the LEED pattern while heating the sample and found the $(\sqrt{2} \times \sqrt{2})R45^\circ$ reconstruction to persist up to at least 500 °C, at which point, the pattern became obscured due to thermal radiation from the sample (data not shown). Therefore, we cannot completely discount the possibility that the $(\sqrt{2} \times \sqrt{2})R45^\circ$ reconstruction is lifted at 700 °C. Under this scenario, APDBs could form when the $(\sqrt{2} \times \sqrt{2})R45^\circ$ renucleates out of phase as the sample is cooled.

The open question from the experimental STM images pertains to the origin of the bright protrusions that are often observed at the APDBs. The observation of missing protrusions [as shown in Fig. 2(b)] indicates the protrusions are not intrinsic to the APDB but may result from an adsorbate preferentially adsorbed at the boundary. The double bright protrusion over the Fe(B) rows closely resembles hydroxyl groups on the regular Fe_3O_4(001) surface[21,30] [one such hydroxyl is indicated by the dashed oval in Fig. 2(b)]. The presence of a surface hydroxyl modifies the density of states (DOS) of the neighboring surface Fe(B) pair, enhancing its contrast in STM.[22,30] The APDB related protrusions have a slightly increased apparent height compared to a hydroxyl species on the regular terrace (ca. 5%), but this may be explained by differences in the electronic structure around the APDB.

B. Computations

Figure 4(a) shows a simulated STM image prepared using the Tersoff-Hamann approximation[44] for the distorted B-layer surface [the converged geometry is shown on the left-hand side of Fig. 1(b)] including bands 0 to 1 eV above the Fermi level. This corresponds to the ca. 1 V empty states used in the experimental STM images of Figs. 2 and 3. This image clearly shows the undulations of the $(\sqrt{2} \times \sqrt{2})R45^\circ$ reconstruction observed experimentally. Calculations for charge-order configurations other than that shown in Fig. 1(b) do not reproduce the characteristic relaxations associated with the distorted B-layer model. For example, one calculation converged to a metastable state with one Fe^{2+} cation in place of a Fe^{3+} cation in the second layer. This resulted in an unreconstructed slab with an increased energy of 0.055 eV [14 meV per surface Fe(B) atom]. These results highlight the sensitivity of the system in the details of the subsurface charge order. Interestingly, the STM simulation shown in Fig. 4(a) results from a surface on which the amplitude of the lattice distortion is only 0.03 Å [this amplitude is shown on the left-hand side of Fig. 1(b)]. This shows that the undulations observed in STM are primarily electronic in nature, consistent with the experimental observation that the amplitude of the undulations depends on the sample bias and is most pronounced in the range of 1–1.2 V.

In Fig. 4(b), we show the charge-order pattern imposed in the second layer of a 3×3 surface unit cell, the minimum size in which an APDB could be modeled. The charge-order pattern

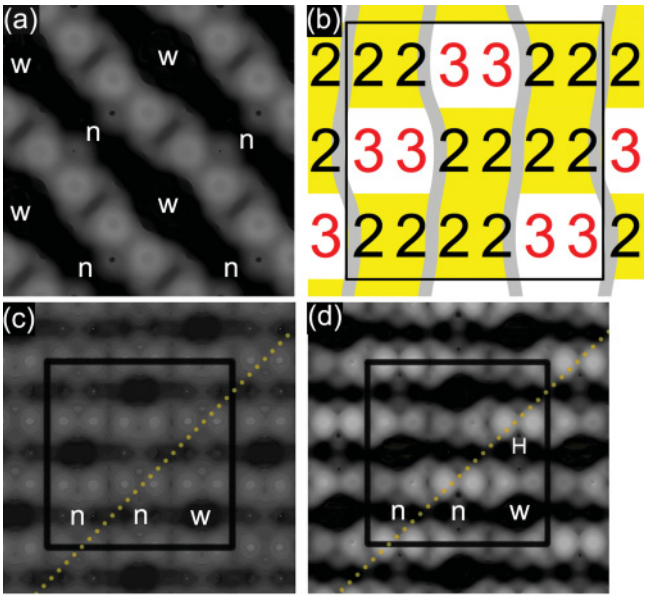

FIG. 4. (Color online) Simulated STM images. (a) A clean surface with a $(\sqrt{2} \times \sqrt{2})R45^\circ$ reconstruction. This image reproduces the undulating rows of Fe(B) atoms as observed experimentally. (b) Schematic of the 3 × 3 unit cell used to calculate the APDB structure. The numbers show the nominal charge state imposed on the second layer Fe(B) atoms using U_{eff}. (c) A clean surface with APDB. This image clearly shows the narrow-narrow junction at the APDB, which is marked by the dashed yellow line. Due to the small unit cell, a periodic array of APDBs is present. (d) A row of hydrogen atoms adsorbed to surface oxygen atoms at the APDB. The adjacent Fe(B) atoms, which reside between the narrow-narrow junction at the APDB, are reduced to Fe^{2+} and appear as bright spots in the simulated STM image.

of the APDB is imposed using the U_{eff} parameter before the system is relaxed. The final structure exhibits an n-n junction above the four Fe^{2+} cations in the subsurface layer, consistent with the APDB in the experimental data [Fig. 2(c)]. A Tersoff-Hamann simulation created from the final converged geometry of the APDB calculation is shown in Fig. 4(c).

Finally, a single-file row of H atoms adsorbed to surface oxygen was studied for three positions near the APDB: (a) as close to the center of the APDB as possible where the narrow-narrow junction occurs, (b) on the narrow side of the narrow-wide junction one row away from the APDB, and (c) on the wide side of the narrow-wide junction one row away from the APDB. Case (a) causes a bright $Fe(B)^{2+}$ pair to be located at the narrow-narrow junction of the APDB. Cases (b) and (c) cause the bright $Fe(B)^{2+}$ pair to be located one Fe(B) row away from the APDB. The DFT + U computed energies showed case (a) is 25 meV per H atom more favorable than case (b), suggesting H adsorption is preferred directly at the narrow-narrow junction. This agrees with the location of bright protrusions along the APDB in the experimental STM images of Fig. 2, and the simulated STM image in Fig. 4(d) is in good agreement with the experimental ones. For adsorption at the adjacent narrow-wide junction, computations showed adsorption in the narrow site [case (b)] was 79 meV per H atom more favorable than adsorption in the wide site [case (c)]. This is consistent with experimental observations that H adsorption on these surfaces (without APDBs) occurs in the narrow site.[22,30] Thus, it seems quite likely that H atom adsorption directly at the narrow-narrow junction is the basis of the bright protrusions along the APDB. Apparently, these do not migrate to the adjacent row because of the energy penalty associated with diffusing away from the APDB.

IV. DISCUSSION

In the preceding section, we have demonstrated the existence of extremely stable APDBs in the $(\sqrt{2} \times \sqrt{2})R45^\circ$ reconstruction of the $Fe_3O_4(001)$ surface. The APDBs are distinct from those that occur during the growth of $Fe_3O_4(001)$ thin films on MgO(001), which are already well characterized and exhibit interesting electronic and magnetic properties.[26–29] Whereas the oxygen sublattice of Fe_3O_4 and MgO are similar (mismatch of 0.3%), facilitating smooth epitaxial growth, the lattice parameter of Fe_3O_4 (8.397 Å) is twice that of the MgO due to the more complicated arrangement of Fe in interstitial sites than exists for Mg. This means that independently nucleated domains of Fe_3O_4 can have one of several registries to the substrate, and when these grow together, there are discontinuities in the Fe sublattice. Such domain boundaries are extremely stable as removing them requires large movements of Fe atoms throughout the structure.

A mismatch between the two components of the system is also responsible for the formation of the APDBs observed at the $Fe_3O_4(001)$ surface. In this case, the size of the $(\sqrt{2} \times \sqrt{2})R45^\circ$ unit cell is the same as that of the bulk structure, but there are two equally likely possibilities for the registry between them. Thus, independently nucleated islands have a 50% chance of being out of phase with one another. When two such islands merge during annealing of the sample, APDBs occur. It is important to note that, in this scenario, there is no discontinuity in the Fe sublattice, merely a discontinuity in the subtle relaxations that make up the lattice distortion. Thus, the stability of the surface APDBs does not arise through the necessity of moving all Fe(B) within a domain but is rather linked to the inherent stability of the $(\sqrt{2} \times \sqrt{2})R45^\circ$ reconstruction.

Extended annealing of the as-prepared surface (12 h at 700 °C) results in no significant difference in the structure or spatial density of APDBs. In order for the APDB to move, the reconstruction has to be lifted locally before it can reform in the opposite phase. Given that the distorted B-layer termination is calculated to be ∼20 meV/Å^2 more stable than an ideal unreconstructed surface,[16] this process presents a significant barrier to APDB diffusion. Furthermore, the APDBs clearly exhibit a preference to form the shortest possible length between step edges under the constraint of their local directions being 45° with respect to the Fe rows, suggesting that that each unit length of APDB costs significant energy. In order to completely remove the APDB, one would first have to extend its length in order for it to reach a second step edge somewhere along its path. Given the large terrace size observed after 700 °C annealing, prohibitively large extensions in length are required, and the APDBs remain.

In this paper, we demonstrate that the distorted B-layer model of the $Fe_3O_4(001)$ surface (see Fig. 2) can be used to interpret the structure of the surface APDBs. Within

this model, the experimentally observed preference for the boundary to occur at a narrow-narrow junction implies that pairs of subsurface Fe^{2+}-like cations meet at the boundary in the subsurface layer. Thus, the APDB represents a disruption in the subsurface charge-order pattern as well as the observed disruption in the undulations of the surface Fe(B) rows [Fig. 2(d)]. DFT + U calculations in which the supposed charge-order pattern is imposed reproduce the narrow junction observed experimentally at the APDB, and simulated STM images are in good agreement with the experimental images. As the structure and properties of the APDB can be reproduced by imposing the charge order on the second B layer alone, we infer that any charge order that may be present on the fourth and deeper B layers has little impact on the surface properties. The third B layer cannot couple to the phase of charge order on the second octahedral layer since the second and third octahedral layers are mutually perpendicular. These results, together with the result that the $(\sqrt{2} \times \sqrt{2})R45^\circ$ reconstruction is inextricably linked to the bimodal charge-order pattern, suggest that understanding the subsurface charge order is critical for understanding the properties of the $Fe_3O_4(001)$ surface.

Both our experimental and theoretical results indicate that the APDB is a preferred site for the adsorption of hydroxyl groups. The presence of an adsorbed H atom causes the nearest surface Fe(B) pair to change from Fe^{3+} to Fe^{2+}, increasing their DOS near the Fermi level, enhancing their contrast in STM.[22,30] Given that the APDB is a comparatively electron-rich area of the surface owing to the excess Fe^{2+} cations beneath, it is somewhat surprising that an electron-donating adsorbate, such as an H atom should preferentially bind there. Nevertheless, this observation is consistent with H atoms adsorbed on the clean surface, which strongly prefer the narrow sites, above Fe^{2+} in the second layer. Interestingly, Fe adatoms, which also could be expected to donate electrons to the system, strongly prefer the narrow sites.[21] Further studies of adsorption at the $Fe_3O_4(001)$ surface will be important to understand how a subtle electronic effect can influence surface processes. The unambiguous nature of the experimental data provides an important benchmark to test the ability of theoretical calculations to model strongly correlated electron systems.

V. CONCLUSIONS

The existence of highly stable APDBs in the distorted B-layer termination of $Fe_3O_4(001)$ was demonstrated by STM. The APDBs most likely form through the merging of smaller terraces during annealing of the sample and exhibit a characteristic structure, running at 45° to the Fe(B) rows. The structure was interpreted using the distorted B-layer model of the $(\sqrt{2} \times \sqrt{2})R45^\circ$ reconstruction, and it was shown that the preference for APDBs to form at narrow-narrow junctions in the surface layer was consistent with a preference for the formation of four-Fe^{2+} cation chains in the subsurface layer. DFT + U calculations show that the distorted B-layer model can be successfully used to model the APDBs with simulated STM images based on the proposed electronic structure reproducing the main features of the experimental data. The results demonstrate the importance of subsurface charge order in the $(\sqrt{2} \times \sqrt{2})R45^\circ$ reconstruction of $Fe_3O_4(001)$ and provide support for the distorted B-layer model of the system.

ACKNOWLEDGMENTS

This material is based on work supported as part of the Center for Atomic Level Catalyst Design, an Energy Frontier Research Center funded by the US Department of Energy, Office of Science, Office of Basic Energy Sciences under Award Number DE-SC0001058 (Center for Atomic Level Catalyst Design). Supercomputing resources were provided by the Georgia Institute of Technology. We thank Zbigniew Łodziana for useful discussions.

*Parkinson@iap.tuwien.ac.at

[1] R. M. Cornell and U. Schwertmann, *The Iron Oxides: Structure, Properties, Reactions, Occurrences and Uses* (Wiley-VCH, Weinheim, 2003).
[2] P. Tartaj, M. P. Morales, T. Gonzalez-Carreño, S. Veintemillas-Verdaguer, and C. J. Serna, Adv. Mater. **23**, 5243 (2011).
[3] E. J. W. Verwey, Nature (London) **144**, 327 (1939).
[4] F. Walz, J. Phys.: Condens. Matter **14**, R285 (2002).
[5] M. Coey, Nature (London) **430**, 155 (2004).
[6] V. V. Shchennikov and S. V. Ovsyannikov, J. Phys.: Condens. Matter **21**, 271001 (2009).
[7] J. Blasco, J. García, and G. Subías, Phys. Rev. B **83**, 104105 (2011).
[8] M. S. Senn, J. P. Wright, and J. P. Attfield, Nature (London) **481**, 173 (2012).
[9] P. Piekarz, K. Parlinski, and A. M. Oleś, Phys. Rev. Lett. **97**, 156402 (2006).
[10] P. Piekarz, K. Parlinski, and A. M. Oleś, Phys. Rev. B **76**, 165124 (2007).
[11] K. Yamauchi, T. Fukushima, and S. Picozzi, Phys. Rev. B **79**, 212404 (2009).
[12] T. Fukushima, K. Yamauchi, and S. Picozzi, J. Phys. Soc. Jpn. **80**, 014709 (2011).
[13] Z. Łodziana, Phys. Rev. Lett. **99**, 206402 (2007).
[14] N. Mulakaluri, R. Pentcheva, M. Wieland, W. Moritz, and M. Scheffler, Phys. Rev. Lett. **103**, 176102 (2009).
[15] N. Mulakaluri, R. Pentcheva, and M. Scheffler, J. Phys. Chem. C **114**, 11148 (2010).
[16] R. Pentcheva, F. Wendler, H. L. Meyerheim, W. Moritz, N. Jedrecy, and M. Scheffler, Phys. Rev. Lett. **94**, 126101 (2005).
[17] R. Pentcheva, W. Moritz, J. Rundgren, S. Frank, D. Schrupp, and M. Scheffler, Surf. Sci. **602**, 1299 (2008).
[18] R. Wiesendanger, I. V. Shvets, D. Bürgler, G. Tarrach, H. J. Güntherodt, J. M. D. Coey, and S. Gräser, Science **255**, 583 (1992).
[19] B. Stanka, W. Hebenstreit, U. Diebold, and S. A. Chambers, Surf. Sci. **448**, 49 (2000).
[20] S. F. Ceballos, G. Mariotto, K. Jordan, S. Murphy, C. Seoighe, and I. V. Shvets, Surf. Sci. **548**, 106 (2004).

[21]G. S. Parkinson, Z. Novotný, P. Jacobson, M. Schmid, and U. Diebold, Surf. Sci. Lett. **605**, L42 (2011).
[22]G. S. Parkinson, Z. Novotný, P. Jacobson, M. Schmid, and U. Diebold, J. Am. Chem. Soc. **133**, 12650 (2011).
[23]A. V. Mijiritskii, M. H. Langelaar, and D. O. Boerma, J. Magn. Magn. Mater. **211**, 278 (2000).
[24]S. A. Chambers, S. Thevuthasan, and S. A. Joyce, Surf. Sci. **450**, L273 (2000).
[25]K. Jordan, A. Cazacu, G. Manai, S. F. Ceballos, S. Murphy, and I. V. Shvets, Phys. Rev. B **74**, 085416 (2006).
[26]R. G. S. Sofin, S. K. Arora, and I. V. Shvets, Phys. Rev. B **83**, 134436 (2011).
[27]D. T. Margulies, F. T. Parker, M. L. Rudee, F. E. Spada, J. N. Chapman, P. R. Aitchison, and A. E. Berkowitz, Phys. Rev. Lett. **79**, 5162 (1997).
[28]F. C. Voogt, T. T. M. Palstra, L. Niesen, O. C. Rogojanu, M. A. James, and T. Hibma, Phys. Rev. B **57**, R8107 (1998).
[29]T. Hibma, F. C. Voogt, L. Niesen, P. A. A. van der Heijden, W. J. M. de Jonge, J. J. T. M. Donkers, and P. J. van der Zaag, J. Appl. Phys. **85**, 5291 (1999).
[30]G. S. Parkinson, N. Mulakaluri, Y. Losovyj, P. Jacobson, R. Pentcheva, and U. Diebold, Phys. Rev. B **82**, 125413 (2010).
[31]P. Mori-Sánchez, A. J. Cohen, and W. Yang, J. Chem. Phys. **125**, 201102 (2006).
[32]T. Heaton-Burgess and W. Yang, J. Chem. Phys. **132**, 234113 (2010).
[33]D. van der Marel and G. A. Sawatzky, Phys. Rev. B **37**, 10674 (1988).
[34]S. L. Dudarev, G. A. Botton, S. Y. Savrasov, C. J. Humphreys, and A. P. Sutton, Phys. Rev. B **57**, 1505 (1998).
[35]T. A. Manz and D. S. Sholl, J. Chem. Theory Comput. **7**, 4146 (2011).
[36]M. J. Wenzel and G. Steinle-Neumann, Phys. Rev. B **75**, 214430 (2007).
[37]V. C. Rakhecha and N. S. Murthy, J. Phys. C: Solid State Phys. **11**, 4389 (1978).
[38]T. A. Manz and D. S. Sholl, J. Chem. Theory Comput. **6**, 2455 (2010).
[39]R. F. W. Bader, P. J. MacDougall, and C. D. H. Lau, J. Am. Chem. Soc. **106**, 1594 (1984).
[40]P. J. MacDougall and R. F. W. Bader, Can. J. Chem. **64**, 1496 (1986).
[41]See Supplemental Material at http://link.aps.org/supplemental/10.1103/PhysRevB.85.195450 for further details of the theoretical calculations.
[42]Available at [ddec.sourceforge.net].
[43]W. Tang, E. Sanville, and G. Henkelman, J. Phys.: Condens. Matter **21**, 084204 (2009).
[44]J. Tersoff and D. R. Hamann, Phys. Rev. Lett. **50**, 1998 (1983).